Supplementary materials

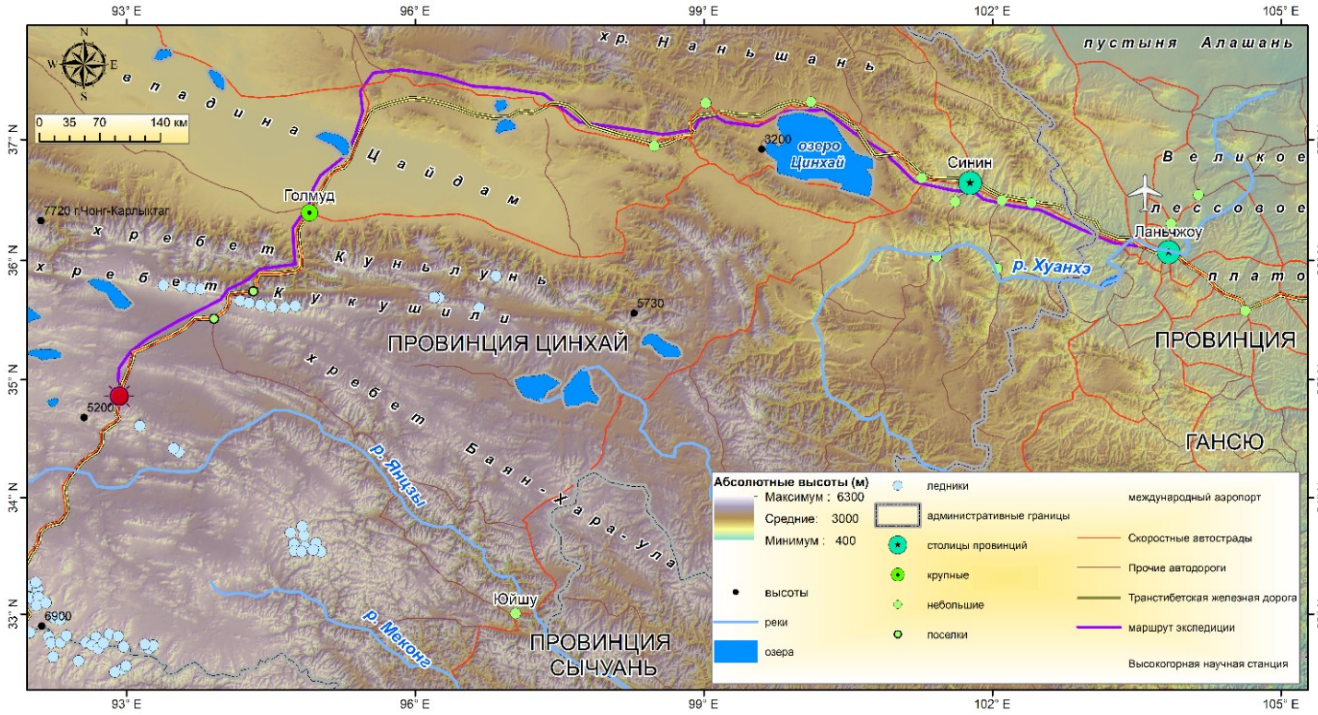

Fig. 1. Location of the study area.

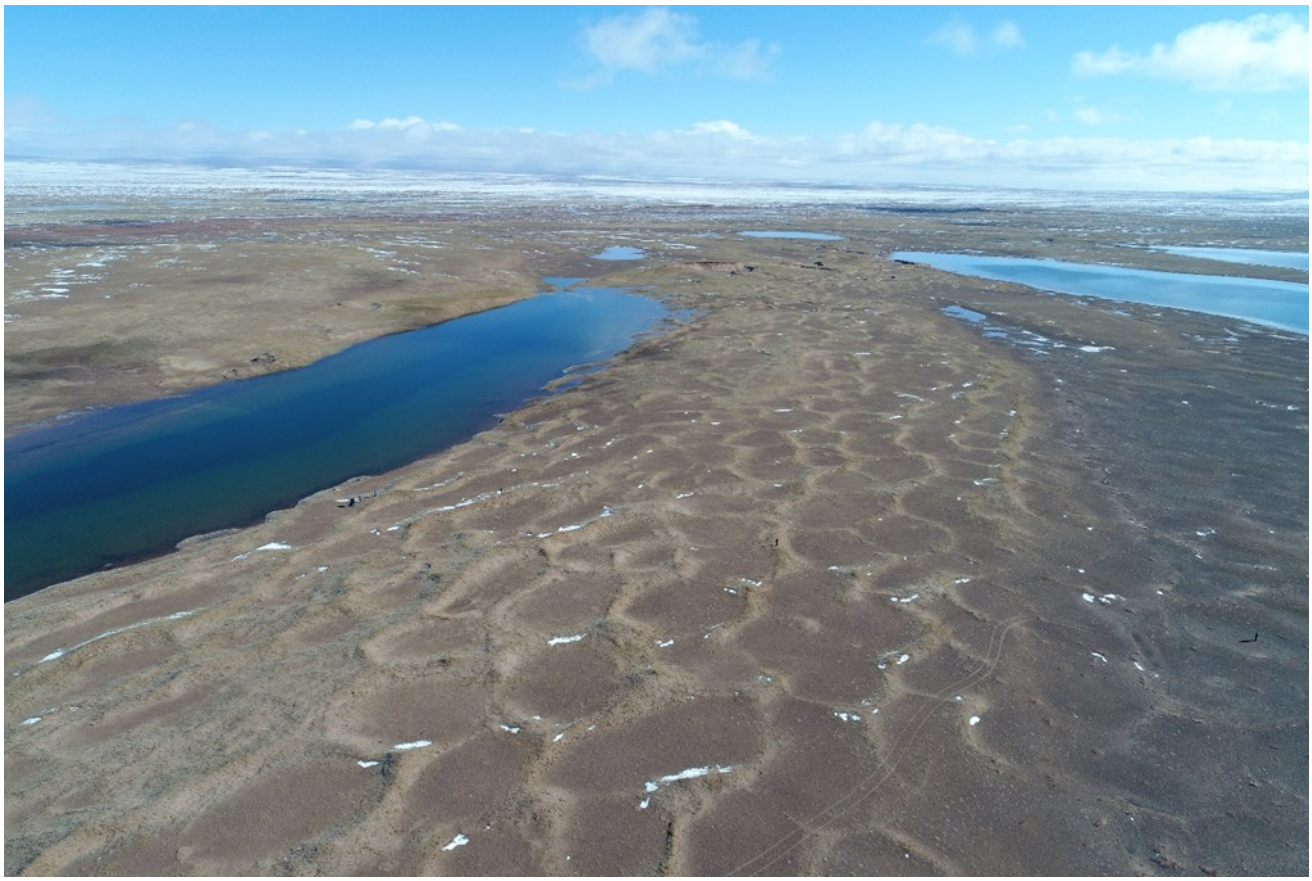

Fig. 2. Polygonal dunes at the study site. Quadcopter survey, October 2018.

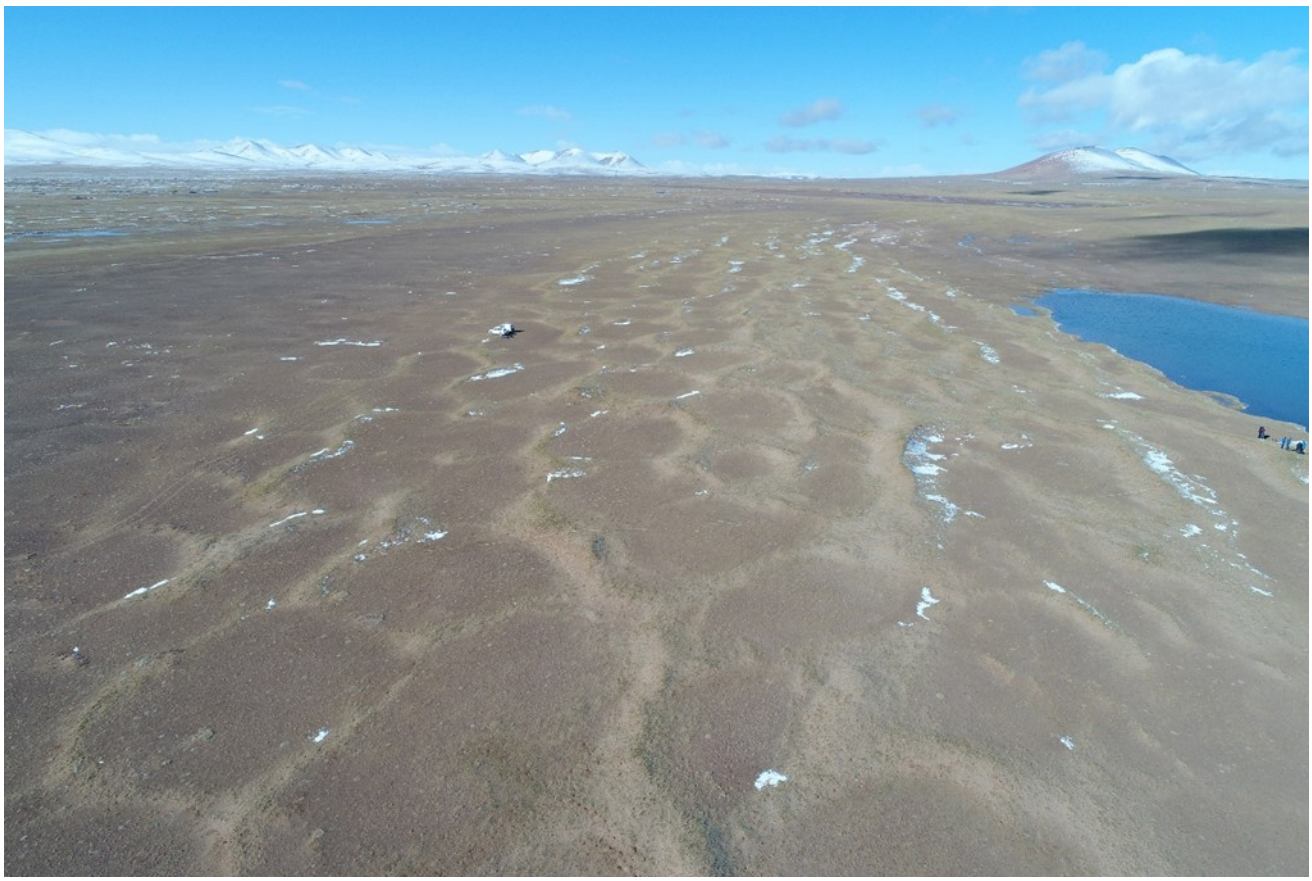

Fig. 3. Polygonal dunes at the study site. Quadcopter survey, October 2018.

Fig. 4. Polygonal dunes at the study site. Quadcopter survey, October 2018.

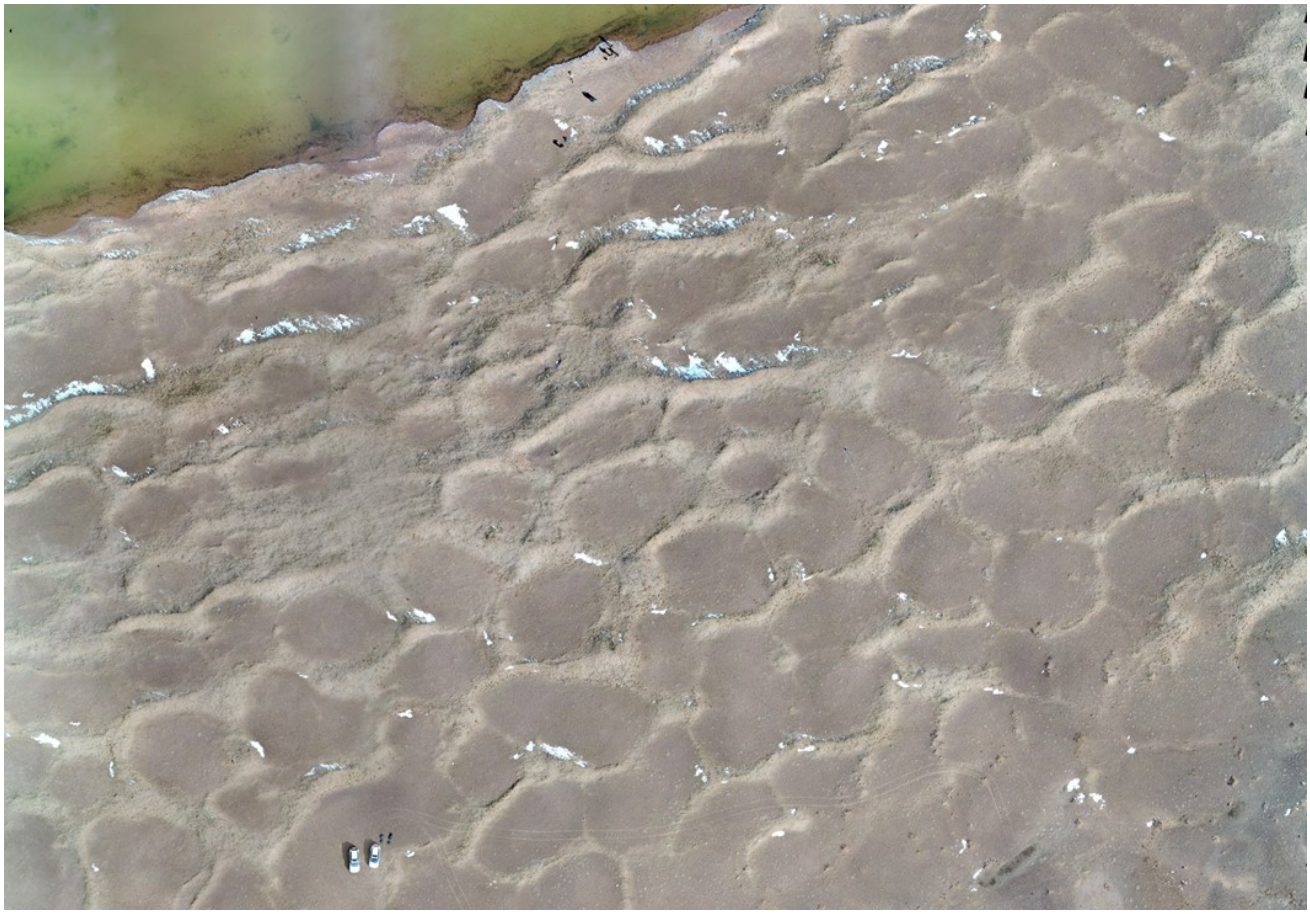

Fig. 5. Polygonal dunes at the study site. Quadcopter survey, orthophoto, October 2018.

Fig. 6. Biogenic-aeolian (sand) mounds in a deflationary basin, October 2018.

Fig. 7. Polygonal dunes at the study site. Quadcopter survey, October 2018.

Fig 8. Partially fixed polygonal sand dunes at the surface of the first terrace of the Beiluhe River, Tibetan Plateau. October 2012. Photo by A.A.Galanin.

Fig. 9. The blow-out in polygonal interdune depressions with single grass curtains at the surface of the first terrace of the Beiluhe River. а – Curtain of Edelweiss alpine (*Leontopodium alpinum*) surrounded by wind eluvium debris, б – carbonate crusts and sinters at the lower surface of debris, в – flattened, aerodynamically shaped ventifacts (swivels), г – classical gabbroid trihedron, д – ventifact with a characteristic “vermiculite” surface structure, е – quartzite ventifact with a finely pitted surface, ж – polished cryptocrystalline green quartzite ventifact.

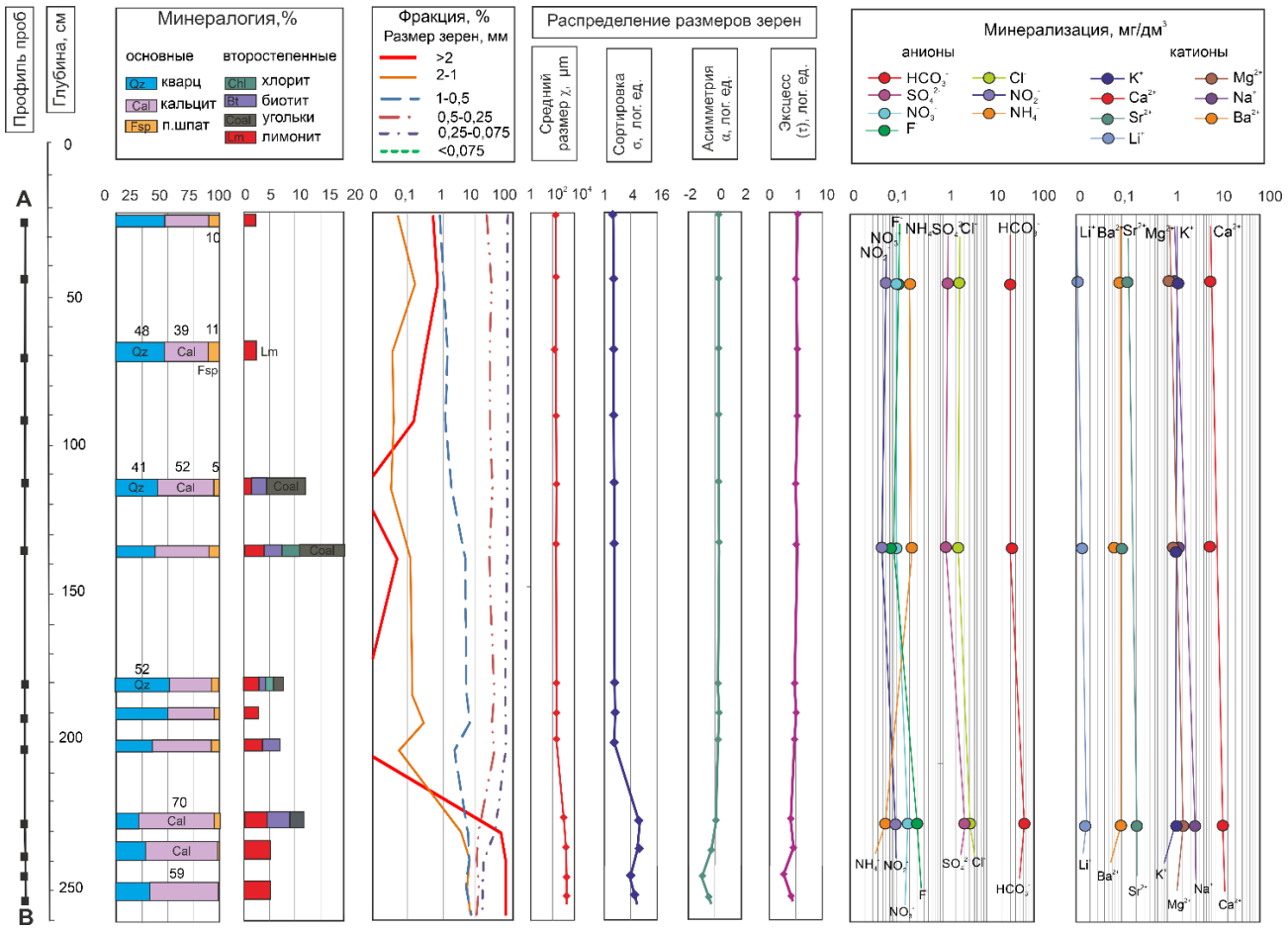

Fig. 10. Variations in mineralogical, grain size, and chemical (soluble components) compositions in the section of the polygonal dune of the 10–12 m wide terrace of the Beiluhe River (Qinghai–Tibet Plateau, clearing C. 432).

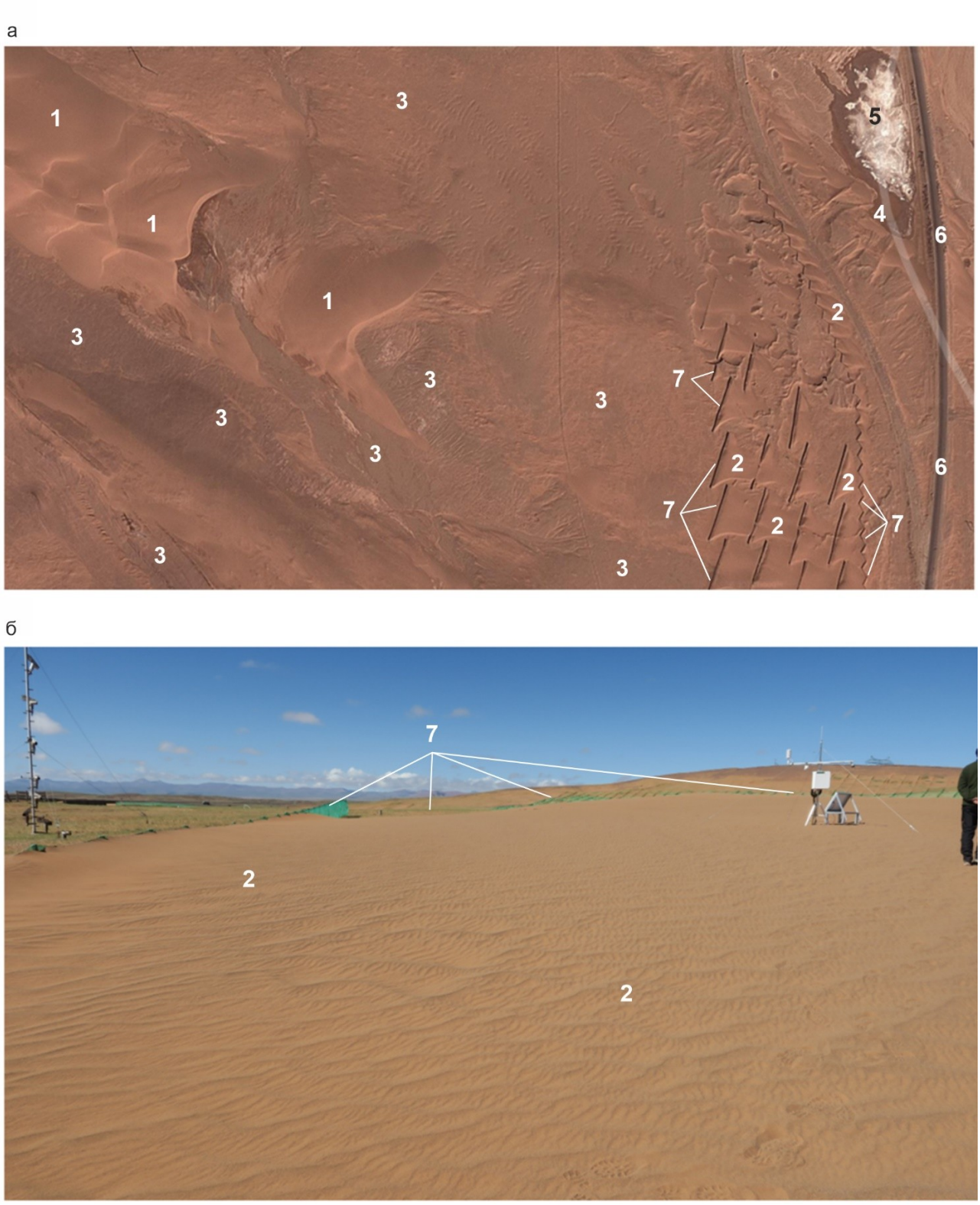

Fig. 11. Recent deflationary-accumulative relief (a) of the high-mountain plain at the headwaters of the Yangtze River (4500 m a.s.l.) and aeolian sand cover at the site with wind-protective mesh fences (b). Sampling point of recent dune sands (Table 1, clearing C. 400). 1 – barkhans, 2 – artificial (shadow) dunes, 3 – deflation areas, 4 – sites of permafrost groundwater discharge, 5 – icing, 6 – Trans-Tibetan Railway, 7 – cascades of wind-protective mesh fences.

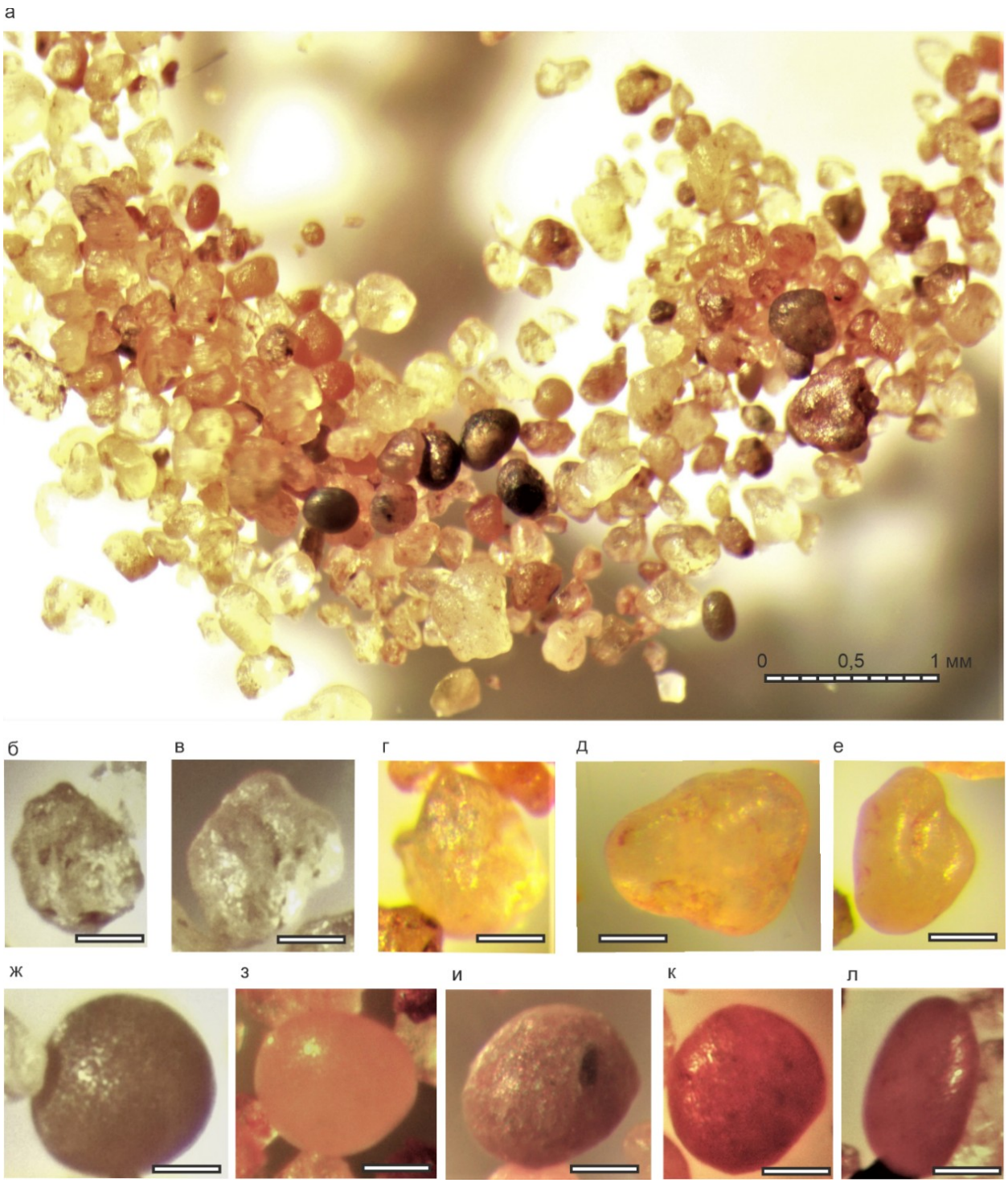

Fig. 12. Dune sand of the 0.2–0.5 mm fraction from the recent aeolian sand covers of the high-elevation plane at the headwaters of the Yangtze River (Tibetan Plateau) under a binocular microscope. Scale bar length is 0.1 mm. а – General view of a random sample; examples of grains of different degrees of roundness and coloration (scale bar is 1 mm): б, в – slightly rounded, uncolored; г – slightly rounded and colored; д, е – well-rounded and colored; ж–л – covered with carbonate glaze, completely rounded (ellipsoids of revolution), and intensely colored.

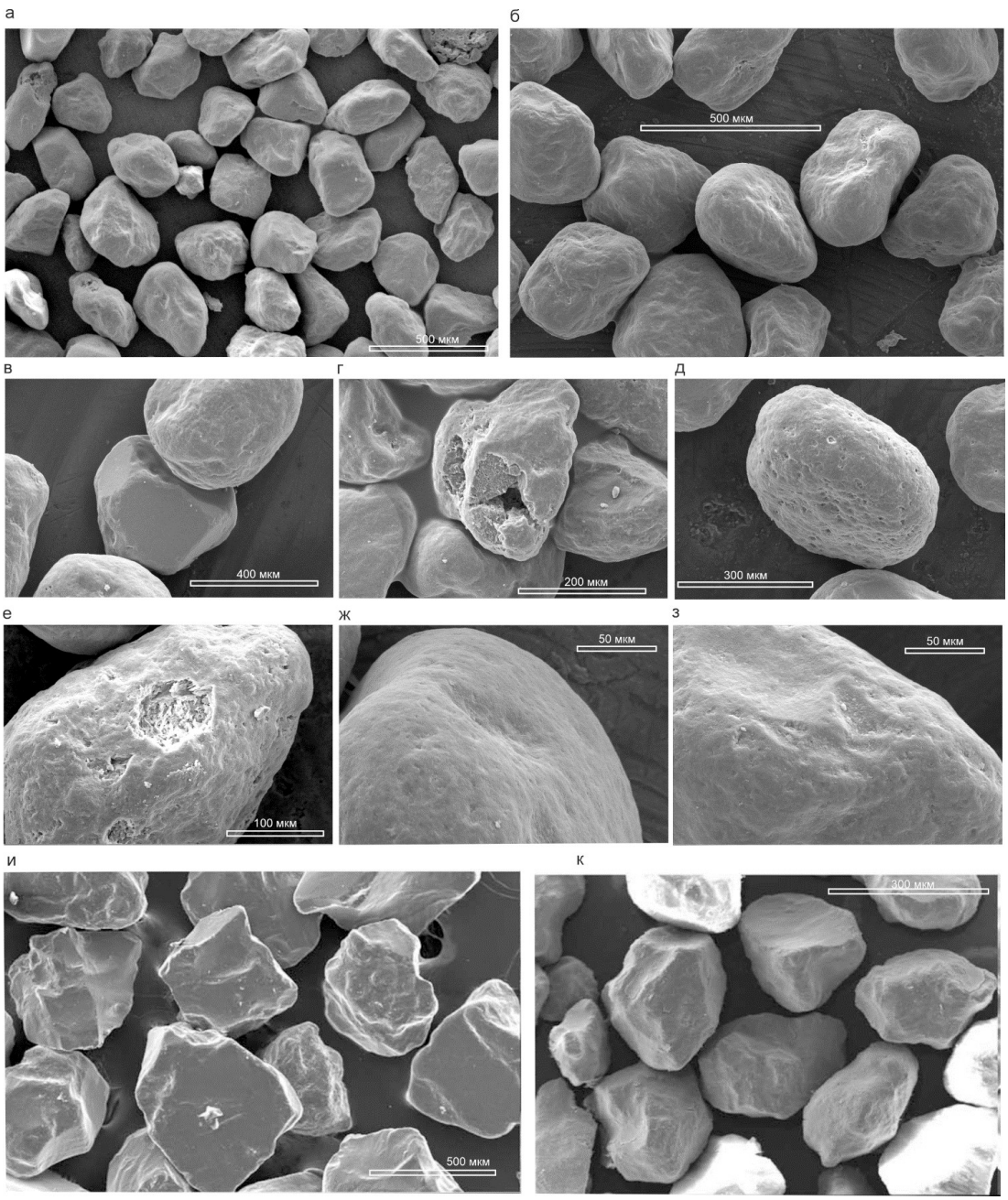

Fig. 13. Quartz grains of the 0.2–0.5 mm fraction from the recent aeolian sand covers of the high-mountain plain at the headwaters of the Yangtze River (Tibetan Plateau) under a scanning microscope. Calcite crusts and glaze were removed by treatment with 5% HCl solution. а, б – General view of a random sample; в – poorly rounded quartz crystal and well-rounded grain; г – agglomerate of grains with voids cemented by insoluble carbonates; д – perfectly rounded grain with a finely pitted surface; е – site of chemical etching at the surface of well-rounded grain; ж – well-rounded grain with a pit; з – rounded grain with a pitted surface and a V-shaped chipping structure; и – unrounded aeolian sand from the recent sand dunes of the Tibetan Plateau (Dong et al., 2017); к – poorly rounded aeolian sand from the giant dunes of the Badyn-Jaran sand sea (Inner Mongolia) (Dong et al., 2017).

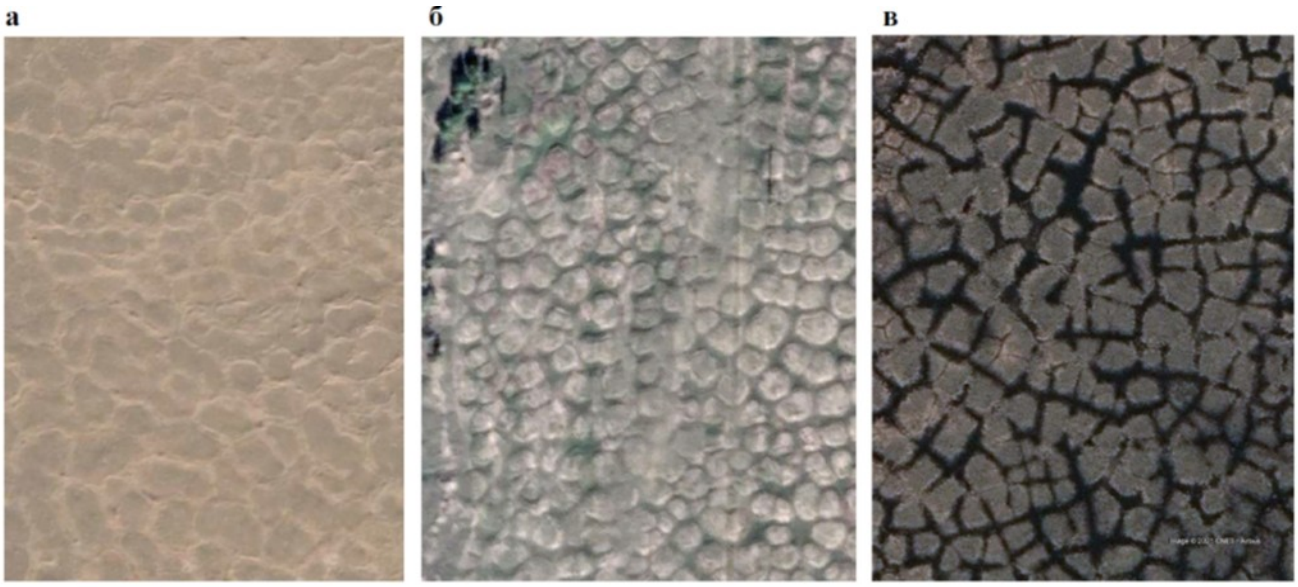

Fig. 14. Similarity between the polygonal pattern of the deflationary-accumulative (polygonal dunes) high-mountain plain at the headwaters of the Yangtze River (а) and the thermal erosion loess–ice (yedoma) plains in the middle reaches of the Lena River (б) and in the lower reaches of the Kolyma River (в). Space images of the Google Earth portal.

Table 1

Grain size composition of the polygonal dunes and underlying alluvium of the 10–12 m wide terrace of the Beiluhe River (Tibetan Plateau), calculated by the modified Folk–Blott geometric method (Folk, 1980; Blott et al., 2001)

Clearing	Member	Facies	Number of samples	Average grain size (x), μm	Sorting factor (σ)	Asymmetry (α)	Kurtosis (τ)	Median (Md), μm	Mode 1, Mode 2, Mode 3, μm
C. 432	II	Weakly fixed polygonal sand dunes	9	200 ± 11	1.62 ± 0.05	0.19 ± 0.03	0.91 ± 0.08	190 ± 9	175
	I	Underlying gravel–pebble–sand alluvium	4	2131 ± 539	5.30 ± 1.05	–0.42 ± 0.43	0.59 ± 0.18	3323 ± 1358	175 325 1500 7500
C. 437	II	Vertical sand vein	2	19 8± 6	1.62 ± 0.,02	0.21 ± 0.,01	0.94 ± 0.08	187 ± 5	175
	I	Host gravel–pebble–sand alluvium	3	1180 ± 641	5.63 ± 0.56	0.23 ± 0.48	0.53 ± 0.07	1160 ± 1361	175 7500 15000
C. 400	II	Recent unfixed cover aeolian sands	7	229 ± 58	1.55 ± 0.10	–0.09 ± 0.17	0.92 ± 0.32	240 ± 68	264 ± 76

Table 2

Mineral composition of the polygonal dunes and underlying alluvium of the 10–12 m wide terrace of the Beiluhe River (Tibetan Plateau)

Clearing	Member	Facies	Number of samples	Examined fraction, mm	Major minerals, %			
					Quartz	Feldspar	Carbonates	Iron hydroxides
C. 432	II	Polygonal sand dunes	5	0.1–0.05	45.8 ± 6.5	7.2 ± 3.3	44.1 ± 6.1	2.9 ± 1.0
	I	Underlying alluvium	4	0.1–0.05	30.4 ± 6.7	3.5 ± 3.6	61.4 ± 7.8	4.7 ± 0.6
C. 437	II	Vertical polygonal sand vein (PSV)	2	0.1–0.05	44.8 ± 6.5	9.1 ± 1.6	44.0 ± 4.7	2.15 ± 0.4
	I	Host alluvium	3	0.1–0.05	39.1 ± 7.8	10.1 ± 1.3	47.8 ± 8.2	3.0 ± 0.8
C. 400	II	Surface of recent dune	1 1 1	0.5–0.25 0.25–0.1 0.1–0.05	63.8 55.4 44.9	1.8 1.1 3.4	34.9 43.5 51.7	– – –

Note. The samples are composed mainly of light-fraction minerals. Heavy fraction is found in single grains and comprises pyroxene, zircon, garnet, amphibole, epidote, and tourmaline. The mineral grains are well rounded or semirounded. Most grains are ferruginized, often with an iron crust at the surface. Some minerals have a carbonate film at the surface.

Table 3

Salt composition of aqueous extract from the polygonal dunes and underlying alluvium of the 10–12 m wide terrace of the Beiluhe River (Tibetan Plateau)

Clearing / Sampling depth, cm	Member	Facies	pH	Eh	Mineralization, mg/dm^3	Content of cations, mg/dm^3						
						Ca^{2+}	Mg^{2+}	Na^{+}	K^{+}	Li^{+}	Sr^{2+}	Ba^{2+}
C. 432/10	II	Duna sand	6.33	500	33.26	8.62	1.30	1.40	1.60	0.01	0.13	0.09
C. 432/180			6.43	487	31.27	7.11	1.43	1.40	1.50	0.02	0.07	0.05
C. 432/225	I	Pebble alluvium	6.83	479	54.60	13.79	1.89	3.50	1.40	0.01	0.19	0,09

Table 3 (continued)

Clearing / Sampling depth, cm	Content of anions, mg/dm^3								
	NH_4^-	HCO_3^-	CO_3^{2-}	SO_4^{2-}	HPO_4^{2-}	Cl^-	F^-	NO_2^-	NO_3^-
C. 432/10	0.22	33.23	0.00	1.30	0.00	2.16	0.10	0.05	0.10
C. 432/180	0.15	32.81	0.00	0.70	0.00	2.55	0.08	0.02	0.22
C. 432/225	0.05	54.69	0.00	3.00	0.00	3.53	0.26	0.10	0.16